A single-phase $Ba_9Lu_2Si_6O_{24}$:Eu^{2+}, Ce^{3+}, Mn^{2+} phosphor with tunable full-color emission for NUV-based white LED applications

Changhua Zhang[a,b], Yongfu Liu[b,*], Jiahua Zhang[c], Xia Zhang[c], Jianxin Zhang[b,d],
Zhixuan Cheng[a,*], Jun Jiang[b,*], Haochuan Jiang[b]

[a] *Department of Chemistry, College of Science, Shanghai University, Shanghai 200444, China*
[b] *Ningbo Institute of Materials Technology and Engineering, Chinese Academy of Sciences, Ningbo 315201, China*
[c] *State Key Laboratory of Luminescence and Applications, Changchun Institute of Optics, Fine Mechanics and Physics, Chinese Academy of Sciences, Changchun 130033, China*
[d] *College of Electronic Information and Engineering, Hangzhou Dianzi University, Hangzhou 10018, China*

ARTICLE INFO

ABSTRACT

We obtained a single phase BLS:Eu^{2+}, Ce^{3+}, Mn^{2+} phosphor by solid-state reactions. Eu^{2+}, Ce^{3+}, and Mn^{2+} gives rise to the blue, green, and red emission, respectively. The Mn^{2+} red emission can be effectively enhanced via energy transfers from both Eu^{2+} and Ce^{3+}. Thus a tunable full color emission from 410 to 750 nm was realized in this single phosphor. The $Eu^{2+} \rightarrow Mn^{2+}$ energy transfer mechanism was investigated by the fluorescence decay curves. This single phosphor exhibits an efficient excitation band covering from 390 to 410 nm, which matches well with the emission light of the efficient NUV chips. The optimized BLS:Eu^{2+}, Ce^{3+}, Mn^{2+} phosphor shows a high quantum efficient of ~62% and a good color stability. When this single phosphor was combined with a 395 nm NUV-chip, an ideal white LED with a high color render index (CRI) of 85 and a correlated color temperature (CCT) of 6300 K was obtained. This demonstrates the promising application of the BLS:Eu^{2+}, Ce^{3+}, Mn^{2+} single phosphor for the NUV-based white LEDs.

1. Introduction

White light-emitting-diodes (WLEDs) are considered to be a promising solid-state lighting source for facilitating the development of society, due to their virtues of energy-saving, environment-friendly, long-lifetime, and high efficiency [1–8]. The most mature method of fabricating WLEDs is the combination of a yellow-emitting YAG:Ce^{3+} phosphor with a blue InGaN chip [9,10]. However, the red emission in YAG:Ce^{3+} is deficient, resulting in the WLED has a low color rendering index (CRI, ~70, ideal = 100) and a high correlated color temperature (CCT, >7000 K). The mixture of red phosphor with yellow or green phosphor for blue-chip-based WLEDs or the mixture of red, green, and blue phosphors for the NUV-chip-based WLEDs can realize an ideal white light with a high CRI and a tunable CCT [11–15]. However, these methods suffer the defect of fluorescence re-absorption among different phosphors, leading to a loss of luminous efficiency and time-dependent color shift. Therefore, it is essential to explore a single phase phosphor with full-color emissions.

Many strategies have been put out to achieve full color emissions in a single phase [16–25]. One kind of the common methods is basing on the NUV-excited phosphors by introducing the red, green, and blue luminescence centers, such as $Ba_3MgSi_2O_8$:Eu^{2+}, Mn^{2+} [26], $Ca_{14}Mg_2[SiO_4]_8$:Eu^{2+}, Mn^{2+} [27], $NaCa_2LuSi_2O_7F_2$:Ce^{3+}, Mn^{2+} [28], $Ca_2SrAl_2O_6$:Ce^{3+}, Li^+, Mn^{2+} [29], and $Mg_2Al_4Si_5O_{18}$:Eu^{2+}, Mn^{2+} [30]. In these systems, Eu^{2+} and Ce^{3+} can be excited by the UV-NUV light and give rise to broad emissions covering from blue to yellow. The Mn^{2+} usually acts as an efficient red-emitting center accompanying with Ce^{3+}/Eu^{2+}. Based on energy transfers mechanisms, many Ce^{3+}/Eu^{2+}/Mn^{2+} co-doped phosphors produce full color emissions.

Alkaline earth silicates are considered as promising hosts for their stable crystal structure and flexible lattice sites. For instance, $Ba_9R_2Si_6O_{24}$ (R = Sc, Y, and Lu) has a rhombohedral crystal structure and can provide multi-occupation sites (Ba and R). For R = Sc and Y, broad emissions covering from green to red can be obtained by codoping Ce^{3+}/Eu^{2+}/Mn^{2+} [31–36]. However, their emissions still lack the blue component and cannot realize an ideal white light. Their quantum efficiency (QE) is also too low (15–47%) [31–33,36].

* Corresponding authors.
E-mail addresses: liuyongfu@nimte.ac.cn (Y. Liu), zxcheng@shu.edu.cn (Z. Cheng), jjun@nimte.ac.cn (J. Jiang).

For R = Lu, that is Ba₉Lu₂Si₆O₂₄ (BLS), we have demonstrated that Eu²⁺ and Ce³⁺ exhibit strong blue and green emissions, respectively, in the BLS host [37]. Codoping Ce³⁺ with Mn²⁺, strong red emissions can be realized in BLS [38]. In this work, we achieve full color emissions, which range from blue to red regions, by codoping Eu²⁺, Ce³⁺, and Mn²⁺ into BLS. Under the 400 nm excitation, the estimated CRI is more than 85 with a CCT of about 6200 K and a QE of about 62%. Combing the single BLS:Eu²⁺, Ce³⁺, Mn²⁺ phosphor with a NUV chip, a WLED with a CRI of 85 and CCT of 6300 K is obtained, which demonstrates the application of this novel phosphor for the NUV-based WLEDs. The ET mechanisms between Eu²⁺ and Mn²⁺ were also investigated in term of fluorescence decays and time-dependent luminescence.

2. Experiment

Samples of BLS:Eu²⁺, BLS:Ce³⁺, BLS:Mn²⁺, BLS:Eu²⁺, Mn²⁺, BLS: Eu²⁺, Ce³⁺, and BLS:Eu²⁺, Ce³⁺, Mn²⁺ were prepared by high temperature solid-state reactions. The starting materials $BaCO_3$ (99.8%), SiO_2 (99.9%), Lu_2O_3 (99.99%), CeO_2 (99.99%), Eu_2O_3 (99.99%), and $MnCO_3$ (99.95%) were weighed in stoichiometric amounts, then mixed and grinded thoroughly in an agate mortar for 40 min. The mixtures were placed in an alumina crucible and sintered in a tube furnace at 1400 °C for 3 h under a reductive atmosphere of 95%N_2 + 5%H_2.

The phases of as-prepared samples were identified by a powder X-ray diffraction (XRD) analysis (Bruker D8), with Cu Kα radiation λ = 1.54056 Å operating at 40 KV, 40 mA and a step size of 2θ = 0.02°. Photoluminescence excitation (PLE) and photoluminescence (PL) spectra at room temperature (RT) were measured by using the Hitachi F-4600 FL spectrometer equipped with a 150 W xenon lamp. The decay curves and the time-resolved PL spectra for Eu²⁺ and Mn²⁺ were recorded on the Horiba Fluorolog Spectrometer (FL3-111) with a 320 nm nanoLED and a 450 W xenon flash lamp excitation sources, respectively. The internal QE, CCT, and CRI from room temperature to 280 °C and the temperature-dependent PL spectra were collected on a quantum efficiency measurement system (Otsuka Photal electronics QE-2100). Prototype WLEDs were fabricated by applying an intimate mixture by weight of the phosphor powder and transparent silicone resin on NUV LED chips (λ_ex = 395 nm). The CRI and CCT of the WLED were measured using the Ocean Optics USB4000 Spectrometer.
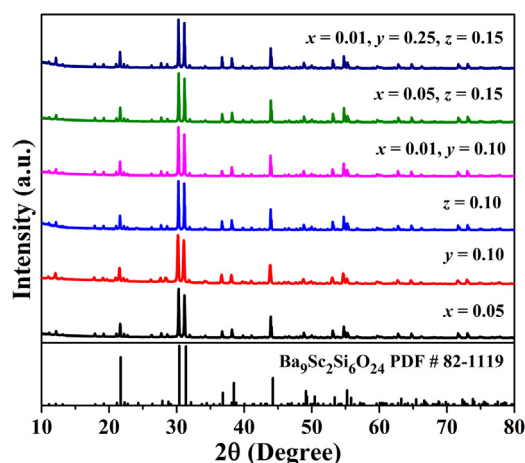
3. Results and discussion

Fig. 1 exhibits the XRD patterns for the Eu²⁺, Ce³⁺, and Mn²⁺ doped or codoped BLS:xEu²⁺, yCe³⁺, zMn²⁺ samples. These samples all exhibit a single phase similar with the BSS (Ba₉Sc₂Si₆O₂₄ PDF # 82-1119) crystal structure [39]. It is clearly that no impure phase was detected. There are three independent barium sites in the BLS host, which are coordinated by 12, 9, and 10 oxygen atoms, respectively, denoted as Ba(1), Ba(2), and Ba(3). The lutetium provides one crystallographic site coordinated with 6 oxygen atoms. In our previous works, we have confirmed that the Eu²⁺ occupies the Ba²⁺ sites while the Ce³⁺ occupies both the Ba²⁺ and Lu³⁺ sites [37]. Mn²⁺ can occupy the Ba²⁺ and Lu³⁺ sites, because the ion radius of Mn²⁺ (0.67 Å) is smaller than that of both Ba²⁺ (1.35 Å) and Lu³⁺ (0.861 Å) [40].

The PLE and PL spectra of BLS:5%Eu²⁺, BLS:10%Ce³⁺, and BLS:10%Mn²⁺ are presented in Fig. 2. As can be seen in Fig. 2(a), the PL spectrum (λ_ex = 400 nm) of BLS:5%Eu²⁺ shows a strong blue emission peaking at 460 nm and a long tail from 460 to 750 nm originating from the df transition of Eu²⁺ at the three different Ba²⁺ sites. The PLE spectrum (λ_em = 460 nm) of BLS:5%Eu²⁺ exhibits a broad excitation band from 240 to 470 nm. In Fig. 2(b), BLS:10%Ce³⁺ shows a broad green emission band peaking at 490 nm, which is ascribed to the df transition of Ce³⁺ at the Lu³⁺ site [37]. The PLE spectrum of BLS:10%Ce³⁺ (λ_em = 490 nm) shows a broad excitation band peaking at 400 nm. These results indicate that the excitation of both BLS:Eu²⁺ and BLS:Ce³⁺ can match well with the emitted light of the efficient NUV chips (390–410 nm). As Fig. 2(c) shows, under 411 nm excitation, BLS:10%Mn²⁺ exhibits a weak red emission peaking at 610 nm, due to the spin-forbidden $^4T_1(^4G) \rightarrow {}^6A_1(^6S)$ transitions of Mn²⁺. The PLE spectrum monitored at 610 nm shows several excitation bands centered at 453, 413, 375, and 326 nm, corresponding to the electronic transitions from the

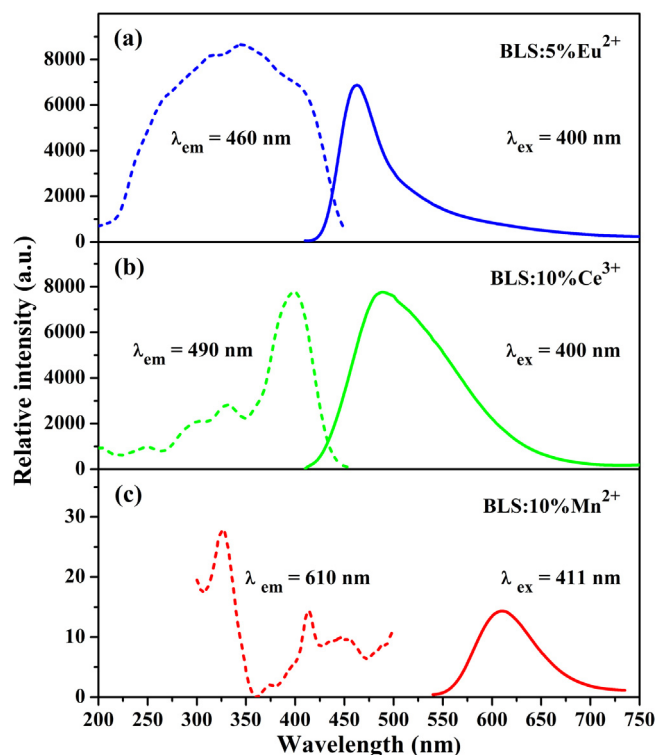**Fig. 1.** XRD patterns for the Eu²⁺, Ce³⁺, and Mn²⁺ doped or codoped BLS:xEu²⁺, yCe³⁺, zMn²⁺ samples.

Fig. 2. PLE and PL spectra of BLS:5%Eu²⁺ (a), BLS:10%Ce³⁺ (b) and BLS:10%Mn²⁺ (c). (For interpretation of the references to color in the text, the reader is referred to the web version of this article.)

$^6A_1(^6S)$ ground state to the excited states of $^4T_1(^4G)$, $[^4A_1(^4G)$, $^4E(^4G)]$, $^4T_2(^4D)$, and $^4E(^4D)$, respectively [41]. It is noted that the PL spectra of both BLS:Eu^{2+} and BLS:Ce^{3+} overlap with the PLE spectrum of BLS:Mn^{2+}, implying the ETs from Eu^{2+} and/or Ce^{3+} to Mn^{2+} can take place. Thus, the Mn^{2+} red emission can be enhanced by codoping Eu^{2+} and/or Ce^{3+} with Mn^{2+} in the BLS matrix. Furthermore, a full-color emission could be obtained by forming the blue, green, and red emission centers in the BLS:Eu^{2+}, Ce^{3+}, Mn^{2+} system. In addition, there is no obvious spectral overlap between Ce^{3+} and Eu^{2+}, which means that no or little ET could happen between them. According to the results above, it should be reasonable to realize a single-composition phosphor with full-color emission for the NUV-based white LEDs.

Fig. 3(a) displays the PL and PLE spectra of BLS:5%Eu^{2+}, zMn^{2+} ($z = 0$, 0.06, 0.10, 0.15, and 0.20). It can be seen that BLS:5%Eu^{2+}, zMn^{2+} exhibits blue-green and red emissions. The blue-green emission intensity of Eu^{2+} decreases monotonically and the red emission increases with increasing Mn^{2+} concentrations, resulting from the Eu$^{2+} \rightarrow$ Mn^{2+} ETs. The red emission includes two parts, one is from the Eu^{2+} emission, and the other is the Mn^{2+} emission. Both of them peak at 610 nm. The inset in Fig. 3(a) presents the normalized PLE spectra of BLS:5%Eu^{2+}, 15%Mn^{2+}. The PLE spectrum for the 610 nm emission has a very similar shape with that for the

510 and 610 nm emissions, suggesting the energy transfer from Eu^{2+} to Mn^{2+} occurs. The lifetime of Eu^{2+} in BLS is determined as 0.600 μs, which is much shorter than that of Mn^{2+} ($\sim$25 ms) in BLS. Therefore, the Mn^{2+} emission in BLS:Eu^{2+},Mn^{2+} can be separated from the Eu^{2+} by the time-resolved spectra [42]. As shown in Fig. 3(b), the red emission of Eu^{2+} (500–750 nm) in the Mn^{2+}-free sample (BLS:5%Eu^{2+}, $z = 0$) has disappeared after a delay time of 50 μs. When Mn^{2+} is codoped into BLS:5%Eu^{2+},zMn^{2+}, the red emissions appears again and reaches a maximum intensity at $z = 0.15$. The maximum of red emissions is same with the results in Fig. 3(a). So, the red emission is ascribed to the Mn^{2+} and the intensity decreases when z exceeds 0.15 due to the Mn^{2+} concentration quenching effect. It is also noticed that the Mn^{2+} red emission band is asymmetry but with a tail from 610 to 750 nm. This indicates that the Mn^{2+} ions should occupy more than one cation sites. Considering that there is only one Lu^{3+} site in BLS, if the red emission is origin from Mn^{2+} at the Lu^{3+} site the PL spectra of Mn^{2+} should be symmetrical. This is not in agreement with the asymmetrical emission bands in Fig. 3(b). BLS has three independent Ba^{2+} sites with different crystal field strength, therefore, the asymmetric red emission should be ascribed to the occupation of Mn^{2+} at the three Ba^{2+} sites. Moreover, the 6-fold Lu^{3+} site has a stronger crystal field-splitting than that of the Ba^{2+} sites, the emission of Mn^{2+} should locate at the near-infrared area if Mn^{2+} occupies at the Lu^{3+} sites. In the inset of Fig. 3(b), the time-resolved PL spectrum of BLS:5%Eu^{2+} exhibits two narrow emission bands peaking at 592 and 613 nm, respectively, which are ascribed to the typical electronic transitions of Eu^{3+} from $^5D_0$ to $^7F_1$ and to $^7F_2$ [43]. The lifetime of Eu^{3+} is about 1–10 ms, so it is reasonable to observe the Eu^{3+} emissions after 50 μs. However, the emission intensity of Eu^{3+} is too weak compared with the red emission of Mn^{2+}, suggesting that there is very little Eu^{3+} in the BLS:Eu^{2+}, Mn^{2+} sample and it will not strongly influence the luminescence properties of Eu^{2+} and Mn^{2+}.

The fluorescence decay curves of Eu^{2+} in BLS:5%Eu^{2+}, zMn^{2+} ($z = 0$–0.20) were measured and presented in Fig. 4(a) and (b). Under the 320 nm excitation, the decay curves of Eu^{2+} monitored at 450 and 500 nm perform multi-exponential decay model. With increasing Mn^{2+} concentrations, the Eu^{2+} decays become faster and faster. The average lifetimes of Eu^{2+} decrease from 596.6 to 559.3 ns and from 618.4 to 557.2 ns, as shown in Fig. 4(c) and (d), respectively. These results strongly demonstrate the Eu$^{2+} \rightarrow$ Mn^{2+} ETs. As known, the ET efficiency, η, can be calculated by the following equation [44]:

$$\eta = 1 - \frac{\tau}{\tau_0}$$

where τ_0 is the intrinsic decay lifetime of Eu^{2+} and τ is the decay time of Eu^{2+} in the presence of Mn^{2+}. η_1 for the 450 nm emission and η_2 for the 500 nm emission were calculated and presented in Fig. 4(e) and (f), respectively. With increasing Mn^{2+} concentrations, both η_1 and η_2 increase and reach 6% and 10% at $z = 0.20$, respectively. Obviously, the ET from the 500 nm green emission is more efficient than from the 450 blue emission. However, the ET efficiency from Eu^{2+} to Mn^{2+} is still too low to enhance the Mn^{2+} red emission strongly. Thus, it is impossible to obtain a white light just based on the BLS:Eu^{2+}, Mn^{2+} system.

Based on the higher ET efficiency from the green emission than that from the blue emission, it is feasible to improve the red emission of Mn^{2+} by enhancing the green emission. We have demonstrated this feasibility in the BLS:Ce^{3+}, Mn^{2+} system, in which strong Mn^{2+} red emissions can be achieved due to the efficient Ce$^{3+} \rightarrow$ Mn^{2+} ETs [36]. However, the luminescence of Ce^{3+} will be affected by Eu^{2+}, because both Eu^{2+} and Ce^{3+} can be effectively excited by the 400 nm. Therefore, it is necessary to determine a suitable Eu^{2+} concentration to ensure an efficient Ce^{3+} emission. Fig. 5 shows the normalized PL spectra of BLS:xEu^{2+}, 10%
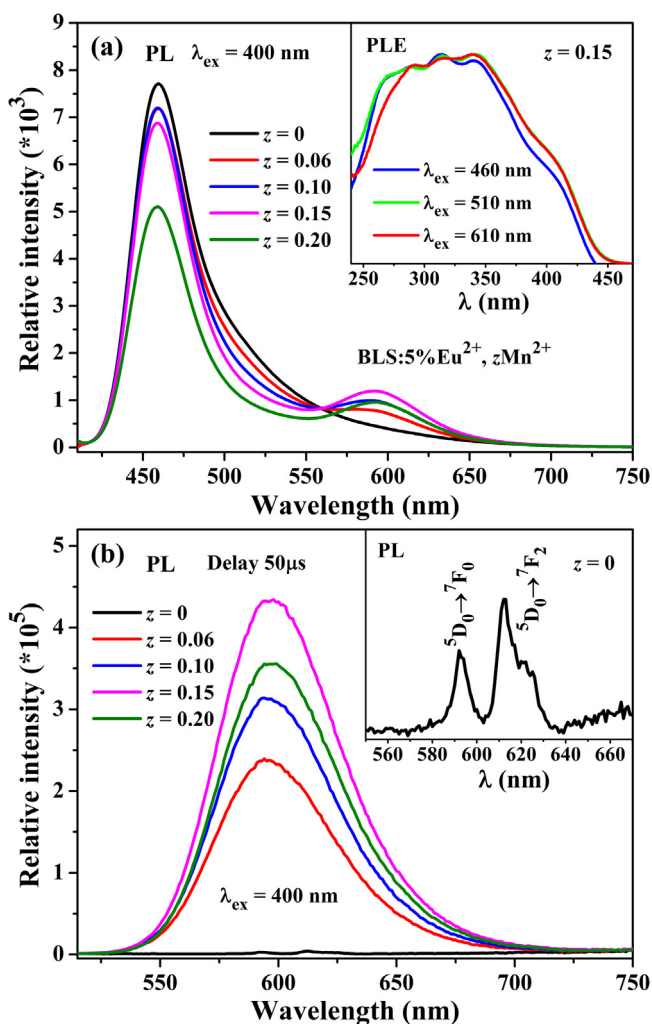

Fig. 3. (a) PL and PLE spectra of BLS:5%Eu^{2+}, zMn^{2+} ($z = 0$–0.20) and (b) time-resolved PL spectra of BLS:5%Eu^{2+}, zMn^{2+} ($z = 0$–0.20) under the 400 nm excitation. (For interpretation of the references to color in the text, the reader is referred to the web version of this article.)
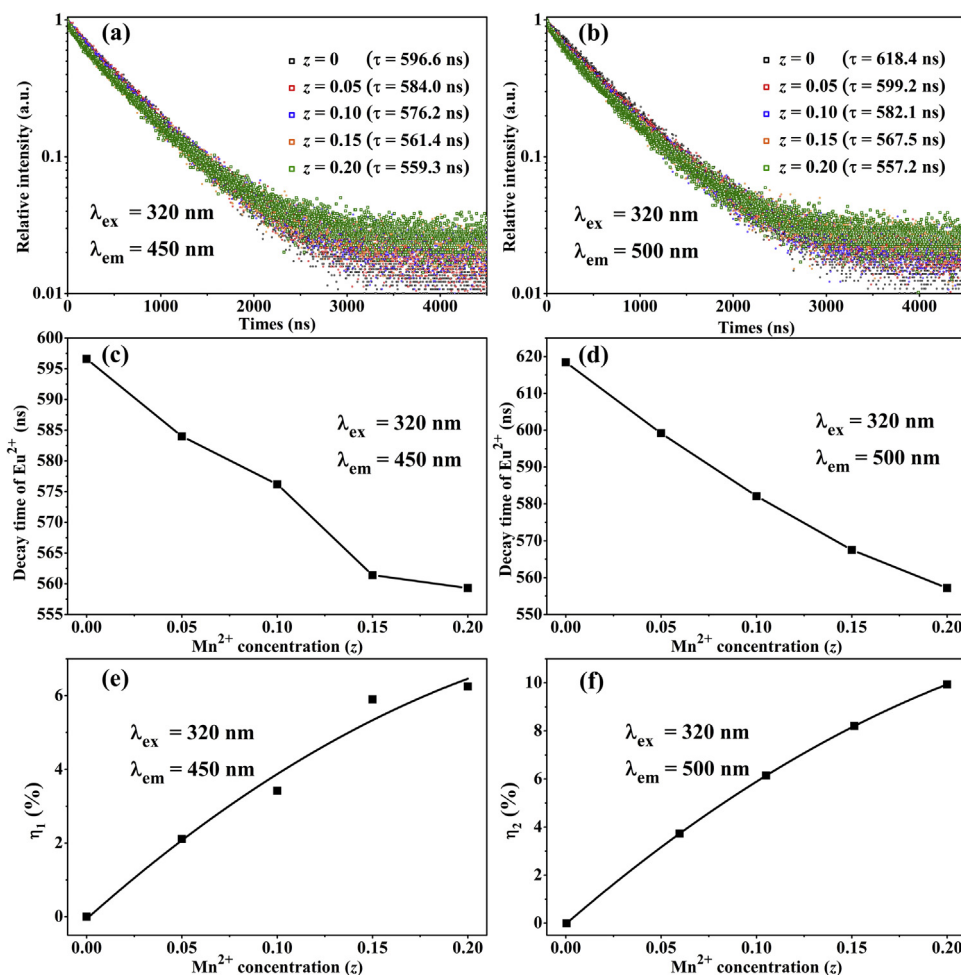
Fig. 4. Fluorescence decay curves of Eu^{2+} in BLS:5%Eu^{2+}, zMn^{2+} (z=0–0.20) monitored at 450 (a) and 500 nm (b) upon 320 nm excitation. Fluorescence lifetimes of Eu^{2+} ((c) and (d)) and ET efficiencies ((e) and (f)) depended on the Mn^{2+} concentrations. (For interpretation of the references to color in the text, the reader is referred to the web version of this article.)

Ce^{3+} (x = 0.01–0.20) under the 400 nm excitation. BLS:1%Eu^{2+}, 10% Ce^{3+} (x = 0.01) exhibits a blue-green emission with a peak at 473 nm, resulting from the overlap of Eu^{2+} and Ce^{3+} emissions.
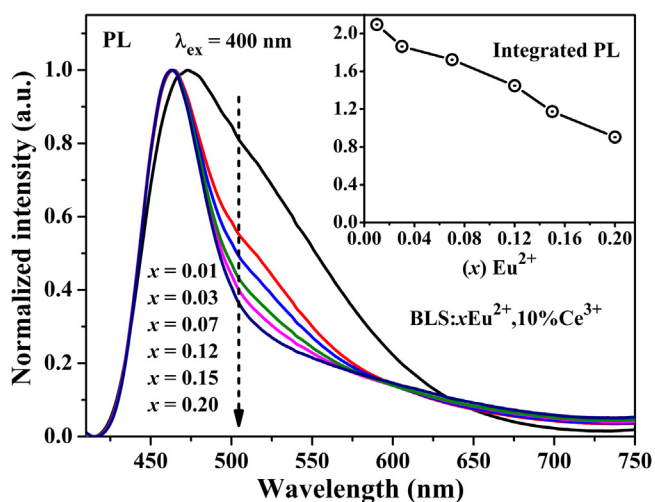

Fig. 5. PL spectra of BLS:xEu^{2+}, 10%Ce^{3+} (x = 0.01-0.20) under the 400 nm excitation. The inset illustrates the integrated PL intensities. (For interpretation of the references to color in the text, the reader is referred to the web version of this article.)

The emission peak shifts from 473 to 460 nm when x exceeds 0.01. Both the green emissions around 500 nm and the integrated PL intensities (the inset) decrease sharply with the increasing Eu^{2+} concentrations. These indicate that the Ce^{3+} green emission will be inhibited when the Eu^{2+} concentration at a high level ($x \geq 0.03$). Thus, to keep efficient Ce^{3+} green emission, a suitable concentration of Eu^{2+} is determined as x = 0.01.

The optimum concentrations of Eu^{2+} and Mn^{2+} have been determined as x = 0.01 and z = 0.15. Accordingly, we optimize the Ce^{3+} concentration to realize an ideal white light emission in the BLS:Eu^{2+}, Ce^{3+}, Mn^{2+} phosphor. As the PL spectra (λ_{ex} = 400 nm) of BLS:1%Eu^{2+},yCe^{3+},15%Mn^{2+} (y = 0.05–0.30) shown in Fig. 6(a), both the green emission around 500 nm and the red emission around 600 nm are improved when the Ce^{3+} concentration exceeds 0.10. Here, Ce^{3+} plays two important roles, one is improving the green emission, and the other is further enhancing the Mn^{2+} red emission by the $Ce^{3+} \rightarrow Mn^{2+}$ ETs. With the Ce^{3+} concentration increases from 0.20 to 0.30, a single white light could be obtained due to the full color emissions. This can be evidenced by the evaluation for the emission spectra and the performance of the phosphor in the NUV-based white LEDs.

Fig. 6(b) depicts the PLE spectra of BLS:1%Eu^{2+}, 25%Ce^{3+}, 15% Mn^{2+} monitored at 460, 490, and 610 nm. For the 460 nm, the PLE spectrum is similar to that of BLS:Eu^{2+}, indicating the blue emission is mainly from Eu^{2+}. However, the excitation peak shifts from 342 to 400 nm, suggesting that the Ce^{3+} luminescence at the
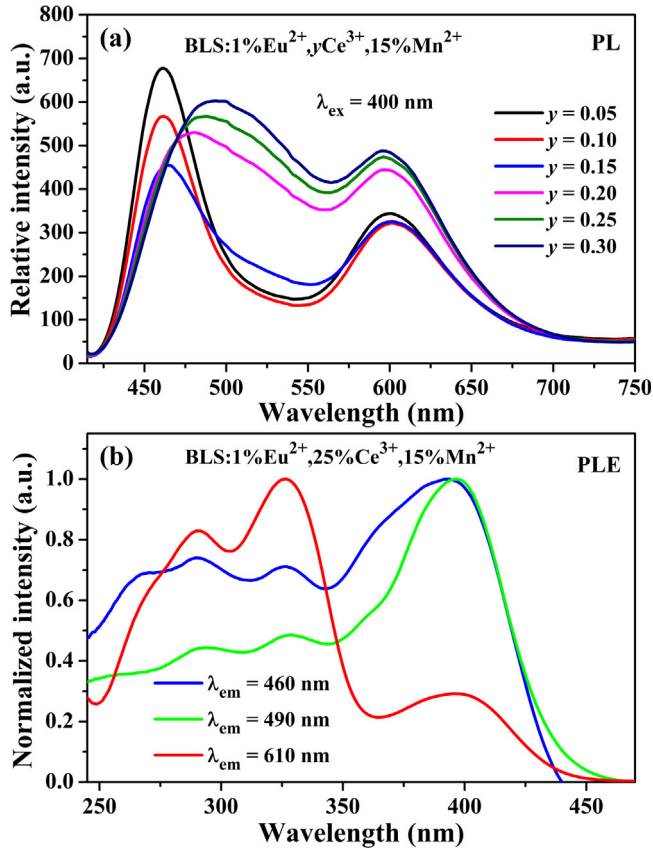
Fig. 7. CIE chromaticity coordinates of the BLS:1%Eu^{2+}, yCe^{3+}, 15%Mn^{2+} samples (y = 0.05–0.30).

Fig. 6. PL spectra of BLS:1%Eu^{2+}, yCe^{3+}, 15%Mn^{2+} (y = 0.05–0.30) under the 400 nm excitation (a). PLE spectra of BLS:1%Eu^{2+}, 25%Ce^{3+}, 15%Mn^{2+} monitored at 460, 490, and 610 nm (b). (For interpretation of the references to color in the text, the reader is referred to the web version of this article.)

Table 1
CCT, CRI, and internal QE for the BLS:1%Eu^{2+}, yCe^{3+}, 15%Mn^{2+} (y = 0.05–0.30) phosphors under the 400 nm excitation.

sample	CCT(K)	CRI	Internal QE (%)
y = 0.05	21500	63.3	53.3
y = 0.10	13450	61.5	47.4
y = 0.15	7860	78.3	50.2
y = 0.20	6610	85.3	54.8
y = 0.25	6260	84.1	61.6
y = 0.30	6210	82.2	60.4

Lu^{3+} site also contributes to the blue emission. For the 490 nm, the PLE spectrum is very close to that of BLS:Ce^{3+}, indicating that the green emission mainly originates from Ce^{3+}. For the 610 nm, the PLE spectrum exhibits a broad excitation band with a peak at 330 nm and a peak at 400 nm, which can be considered as the PLE spectral overlap between BLS:Ce^{3+} and BLS:Eu^{2+}. This also suggests that the Mn^{2+} red emission is enhanced by both the Eu^{2+} → Mn^{2+} and Ce^{3+} → Mn^{2+} ETs.

Fig. 7 illustrates the CIE chromaticity coordinates of BLS:1%Eu^{2+}, yCe^{3+}, 15%Mn^{2+} based on the PL spectra in Fig. 6(a). The coordinates shift from (0.284, 0.228) to (0.314, 0.375) with y increasing from 0.05 to 0.30. It is also clear that a white color can be obtained based on the tunable emissions. The CCT, CRI, and internal QE for the samples were measured and listed in Table 1. Clearly, the CRI of the white light based on the BLS:Eu^{2+}, Ce^{3+}, Mn^{2+} phosphor can reach as high as 85.3 and the internal QE can reach 61.6% for y = 0.25. Here, the temperature-dependent luminescence for the BLS:1%Eu^{2+}, 25%Ce^{3+}, 25%Mn^{2+} were measured. As shown in Fig. 8, at 160 °C, only 58% of the PL intensity at RT is maintained, which exhibits a strong thermal quenching properties. However, the CRI and CCT have little changes with the increasing temperatures, showing good color stability. The Chromaticity Shifts (ΔE) of BLS:1%Eu^{2+}, 25%Ce^{3+}, 25%Mn^{2+} at 373 K and 498 K were calculated according to the following equation [45]:

$$\Delta E = \sqrt{\left(u_t' - u_0'\right)^2 + \left(v_t' - v_0'\right)^2 + \left(w_t' - w_0'\right)^2}$$

where $u' = 4x/(3 - 2x + 12y)$, $v' = 9y/(3 - 2x + 12y)$, and $w' = 1 - u' - v'$; x and y are the chromaticity coordinates in CIE
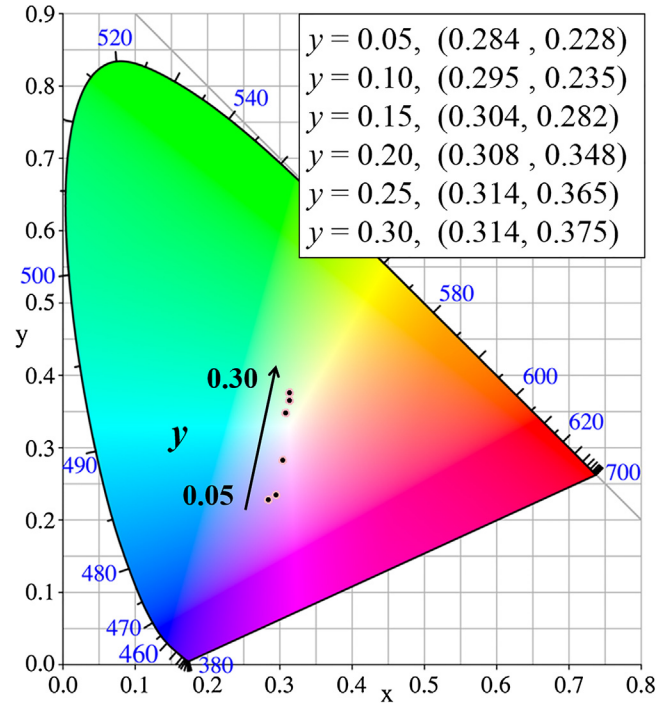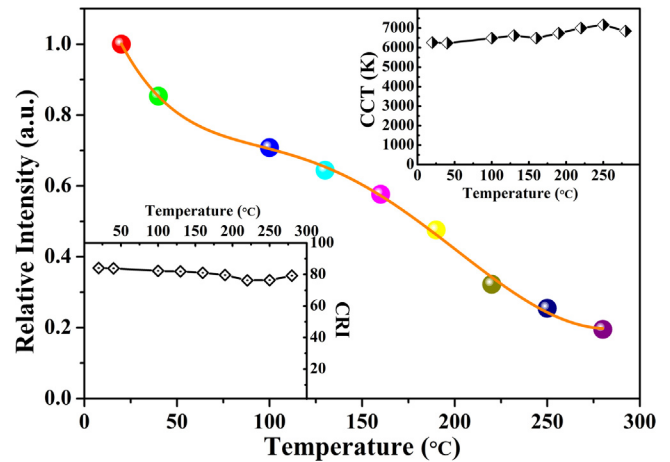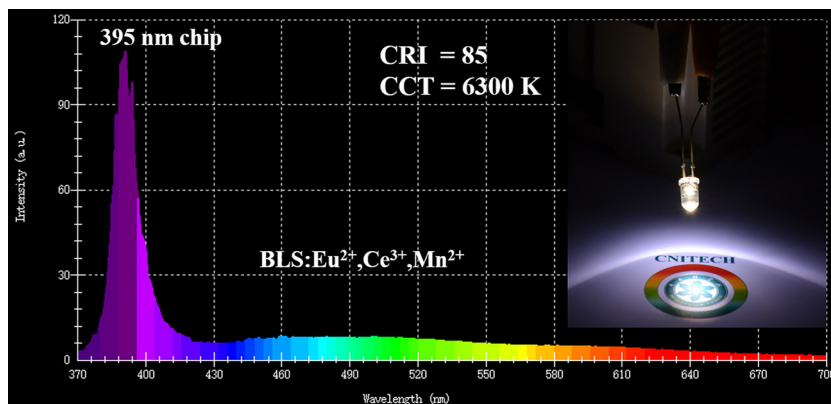

Fig. 8. Temperature-dependent PL intensities of BLS:1%Eu^{2+}, 25%Ce^{3+}, 15%Mn^{2+} under 400 nm excitation. The insets are the CCT (top right) and the CRI (bottom left).

1931, u' and v' are chromaticity coordinates in $u'v'$ uniform color space, 0 and t are the chromaticity shift at 298 K and a given temperature, respectively. As Table 2 lists, the chromaticity shifts of BLS:1%Eu^{2+}, 25%Ce^{3+}, 25%Mn^{2+} at 373 K and 498 K are

Table 2
Chromaticity shifts (ΔE) of BLS:1%Eu^{2+}, 25%Ce^{3+}, 15%Mn^{2+} and commercial white-emitting phosphor mixture at 373 K and 498 K.

Sample	λ_{ex} (nm)	ΔE 373 K	ΔE 498 K
BLS:1%Eu^{2+}, 25%Ce^{3+}, 15%Mn^{2+}	400	0.0065	0.0169
commercial white-emitting phosphor mixture[23]	370	0.0179	0.0522

Fig. 9. Electroluminescence spectra of the WLED device fabricated using a 395 nm NUV-chip and the BLS:Eu^{2+}, Ce^{3+}, Mn^{2+} single phosphor. Inset is the photograph of the corresponding WLED.

0.0065 and 0.0169, respectively, which is only one-third of the commercial white-emitting phosphor mixture at corresponding temperature [23]. These results indicate BLS:1%Eu^{2+}, 25%Ce^{3+}, 25% Mn^{2+} is a potential single phosphor for high-quality NUV-based white LEDs.

Fig. 9 shows the electroluminescence spectra of the fabricated WLED combining the BLS:Eu^{2+}, Ce^{3+}, Mn^{2+} single phosphor with a 395 nm-NUV chip. White light with a high CRI of 85 is obtained due to the full color emission of this single phosphor. The insert photograph of the WLED gives rise to a white light with a CCT of 6300 K. These results demonstrate the good performance and the applications of the BLS:Eu^{2+}, Ce^{3+}, Mn^{2+} single phosphor for the NUV-based WLEDs.

4. Conclusions

In summary, we have successfully synthesized a single phase BLS:Eu^{2+}, Ce^{3+}, Mn^{2+} phosphor by solid-state reactions. The blue, green, and red emission centers were introduced into the BLS host by codoping Eu^{2+}, Ce^{3+}, and Mn^{2+}, respectively. The Eu$^{2+} \rightarrow$ Mn^{2+} ETs were demonstrated by the fluorescence decay curves of Eu^{2+}. The Mn^{2+} red emission were effectively enhanced via ETs from both Eu^{2+} and Ce^{3+}. Thus a tunable full color emission was realized in this single phosphor. Moreover, this single phosphor exhibits an efficient excitation band covering from 390 to 410 nm, which matches well with the emission light of the efficient NUV chips. The optimized BLS:Eu^{2+}, Ce^{3+}, Mn^{2+} phosphor shows a high QE of ~62% and a good color stability. When this single phosphor was combined with a 395 nm NUV-chip, an ideal white LED with a high CRI of 85 and a CCT of 6300 K was obtained. The results demonstrate the promising application of the BLS:Eu^{2+}, Ce^{3+}, Mn^{2+} single phosphor for the NUV-based white LEDs.

References

[1] E.F. Schubert, J.K. Kim, Solid-state light sources getting smart, Science 308 (2005) 1274–1278.

[2] S. Pimputkar, J.S. Speck, S.P. DenBaars, S. Nakamura, Prospects for LED lighting, Nat. Photon. 34 (2009) 180–182.

[3] H. Daicho, T. Iwasaki, K. Enomoto, Y. Sasaki, Y. Maeno, Y. Shinomiya, E. Nishibori, M. Sakata, H. Sawa, S. Matsuishi, H. Hosono, A novel phosphor for glareless white light-emitting diodes, Nat. Commun. 3 (2012) 1132.

[4] J.Y. Tsao, M.H. Crawford, M.E. Coltrin, A.J. Fischer, D.D. Koleske, G.S. Subramania, G.T. Wang, J.J. Wierer, R.F. Karlicek, Toward smart and ultra-efficient solid-state lighting, Adv. Opt. Mater. 2 (2014) 809–836.

[5] J. Meyer, F. Tappe, Photoluminescent materials for solid-state lighting: state of the art and future challenges, Adv. Opt. Mater. 3 (2014) 424–430.

[6] Y. Liu, X. Zhang, Z. Hao, W. Lu, X. Liu, X. Wang, J. Zhang, Crystal structure and luminescence properties of (Ca$_{2.94-x}$Lu$_x$Ce$_{0.06}$)(Sc$_{2-y}$Mg$_y$)Si$_3$O$_{12}$ phosphors for white LEDs with excellent color rendering and high luminous efficiency, J. Phys. D Appl. Phys. 44 (2011) 075402.

[7] Y. Liu, X. Zhang, Z. Hao, Y. Luo, X. Wang, J. Zhang, Crystal structure and luminescence properties of Lu^{3+} and Mg^{2+} incorporated silicate garnet [Ca$_{3-(x+0.06)}$Lu$_x$Ce$_{0.06}$)(Sc$_{2-y}$Mg$_y$)Si$_3$O$_{12}$, J. Lumin. 132 (2012) 1257–1260.

[8] X. Zhang, Y. Liu, Z. Hao, Y. Luo, X. Wang, J. Zhang, Yellow emitting (Ca$_2$Lu$_{1-x}$Ce$_x$)(ScMg)Si$_3$O$_{12}$ phosphor and its application for white LEDs, Mater. Res. Bull. 47 (2012) 1149–1152.

[9] P. Schlotter, R. Schmidt, J. Schneider, Luminescence conversion of blue light emitting diodes, Appl. Phy. A 64 (1997) 417–418.

[10] V. Bachmann, C. Ronda, A. Meijerink, Temperature quenching of yellow Ce^{3+} luminescence in YAG:Ce, Chem. Mater. 21 (2009) 2077–2084.

[11] Y.C. Wu, D.Y. Wang, T.M. Chen, C.S. Lee, K.J. Chen, H.C. Kuo, A novel tunable green-to yellow-emitting β-YFS:Ce^{3+} phosphor for solid-state lighting, ACS Appl. Mater. Interfaces 3 (2011) 3195–3199.

[12] T. Suehiro, R.J. Xie, N. Hirosaki, Facile synthesis of (Sr,Ca)$_2$Si$_5$N$_8$:Eu^{2+}-based red-emitting phosphor for solid-state lighting, Ind. Eng. Chem. Res. 52 (2013) 7453–7456.

[13] S.P. Lee, T.S. Chan, T.M. Chen, Novel reddish-orange-emitting BaLa$_2$Si$_2$S$_8$:Eu^{2+} thiosilicate phosphor for LED lighting, ACS Appl. Mater. Interfaces 7 (2014) 40–44.

[14] P. Pust, A.S. Wochnik, E. Baumann, P.J. Schmidt, D. Wiechert, C. Scheu, W. Schnick, Ca[LiAl$_3$N$_4$]:Eu^{2+} a narrow-band red-emitting nitridolithoaluminate, Chem. Mater. 26 (2014) 3544–3549.

[15] N. Komuro, M. Mikami, Y. Shimomura, E.G. Bithell, A.K. Cheetham, Synthesis: structure and optical properties of cerium-doped calcium barium phosphate—

a novel blue-green phosphor for solid-state lighting, J. Mater. Chem. C 3 (2015) 204–210.

[16] Y. Liu, X. Zhang, Z. Hao, X. Wang, J. Zhang, Tunable full-color-emitting $Ca_3Sc_2Si_3O_{12}$:Ce^{3+}, Mn^{2+} phosphor via charge compensation, Chem. Commun. 47 (2011) 10677–10679.

[17] Y. Liu, X. Zhang, Z. Hao, Y. Luo, X. Wang, J. Zhang, Generating yellow and red emissions by co-doping Mn^{2+} to substitute for Ca^{2+} and Sc^{3+} in $Ca_3Sc_2Si_3O_{12}$: Ce^{3+} green emitting phosphor for white LED applications, J. Mater. Chem. 21 (2011) 16379–16384.

[18] Y. Liu, X. Zhang, Z. Hao, X. Wang, J. Zhang, Generation of broadband emission by incorporating N^{3-} into $Ca_3Sc_2Si_3O_{12}$:Ce^{3+} garnet for high rendering white LEDs, J. Mater. Chem. 21 (2011) 6354–6358.

[19] X. Li, J.D. Budai, F. Liu, J.Y. Howe, J. Zhang, X.J. Wang, Z. Pan, New yellow $Ba_{0.93}Eu_{0.07}Al_2O_4$ phosphor for warm-white light-emitting diodes through single-emitting-center conversion, Light Sci. Appl. 2 (2013) e50.

[20] M. Shang, C. Li, J. Lin, How to produce white light in a single-phase host? Chem. Soc. Rev. 43 (2014) 1372–1386.

[21] W. Lü, Y. Jia, Q. Zhao, W. Lv, H. You, Design of a luminescence pattern via altering the crystal structure and doping ions to create warm white LEDs, Chem. Commun. 50 (2014) 2635–2637.

[22] J. Qiao, J. Zhang, X. Zhang, Z. Hao, Y. Liu, Y. Luo, The energy transfer and effect of doped Mg^{2+} in $Ca_3Sc_2Si_3O_{12}$:Ce^{3+}, Pr^{3+} phosphor for white LEDs, Dalton Trans. 43 (2014) 4146–4150.

[23] X. Zhang, H. Lin, F. Pan, M. Wu, J. Wang, Y. Chen, Q. Su, Highly thermally stable single-component white-emitting silicate glass for organic-resin-free white-light-emitting diodes, ACS Appl. Mater. Interfaces 6 (2014) 2709–2717.

[24] X. Zhang, J. Yu, J. Wang, C. Zhu, J. Zhang, R. Zou, B. Lei, Y. Liu, M. Wu, Facile preparation and ultrastable performance of single-component white-light-emitting phosphor-in-glass used for high-power warm white LEDs, ACS Appl. Mater. Interfaces 7 (2015) 28122–28127.

[25] P. Dai, C. Li, X. Zhang, J. Xu, X. Chen, X. Wang, Y. Jia, X. Wang, Y. Liu, A single-$Eu^2$$^+$-activated high-color-rendering oxychloride white-light phosphor for white-light-emitting diodes, Light Sci. Appl. 5 (2016) e16024.

[26] J.S. Kim, P.E. Jeon, J.C. Choi, H.L. Park, S.I. Mho, G.C. Kim, Warm-white-light emitting diode utilizing a single-phase full-color $Ba_3MgSi_2O_8$: Eu^{2+}, Mn^{2+} phosphor, Appl. Phys. Lett. 84 (2004) 2931–2933.

[27] K.H. Lee, S. Choi, H.K. Jung, W.B. Im, Bredigite-structure $Ca_{14}Mg_2[SiO_4]_8$:Eu^{2+}, Mn^{2+}: a tunable green-red-emitting phosphor with efficient energy transfer for solid-state lighting, Acta Mater. 60 (2012) 5783–5790.

[28] W. Lv, W. Lü, N. Guo, Y. Jia, Q. Zhao, M. Jiao, B. Shao, H. You, Crystal structure and luminescent properties of a novel high efficiency blue-orange emitting $NaCa_2LuSi_2O_7F_2$:Ce^{3+}, Mn^{2+} phosphor for ultraviolet light-emitting diodes, Dalton Trans. 42 (2013) 13071–13077.

[29] M. Jiao, Y. Jia, W. Lü, W. Lv, Q. Zhao, B. Shao, H. You, A single-phase white-emitting $Ca_2SrAl_2O_6$:Ce^{3+}, Li^+, Mn^{2+} phosphor with energy transfer for UV-excited WLEDs, Dalton Trans. 43 (2014) 3202–3209.

[30] J. Chen, Y. Liu, M. Fang, Z. Huang, Luminescence properties and energy transfer of Eu/Mn-coactivated $Mg_2Al_4Si_5O_{18}$ as a potential phosphor for white-light LEDs, Inorg. Chem. 53 (2014) 11396–11403.

[31] L. Bian, T.L. Zhou, J.J. Yang, Z. Song, Q.L. Liu, Crystal structure and photoluminescence of $(Ba_{1-x-y}Sr_yEu_x)_9Sc_2Si_6O_{24}$, J. Lumin. 132 (2012) 2541–2545.

[32] J. Brgoch, C.K. Borg, K.A. Denault, S.P. DenBaars, R. Seshadri, Tuning luminescent properties through solid-solution in $(Ba_{1-x}Sr_x)_9Sc_2Si_6O_{24}$:$Ce^{3+}$, Li^+, Solid State Sci. 18 (2013) 149–154.

[33] Y. Kim, S. Park, Preparation and luminescent properties of Eu-substituted barium–yttrium orthosilicate phosphors, Opt. Mater. 36 (2013) 458–462.

[34] Y. Kim, S. Park, Eu^{2+}, Mn^{2+} co-doped $Ba_9Y_2Si_6O_{24}$ phosphors based on near-UV-excitable LED lights, Mater. Res. Bull. 49 (2014) 469–474.

[35] S. Park, Ce^{3+}-Mn^{2+} cooperative $Ba_9Y_2Si_6O_{24}$ orthosilicate phosphors, Mater. Lett. 135 (2014) 59–62.

[36] L. Bian, C.W. Liu, J. Gao, X.P. Jing, Energy transfer and color tuning in the $Ba_9Sc_2Si_6O_{24}$:Ce^{3+}, Eu^{2+}, Mn^{2+} phosphor, RSC Adv. 5 (2015) 69458–69465.

[37] Y. Liu, J. Zhang, C. Zhang, J. Xu, G. Liu, J. Jiang, H. Jiang, $Ba_9Lu_2Si_6O_{24}$:Ce^{3+}: an efficient green phosphor with high thermal and radiation stability for solid-state lighting, Adv. Opt. Mater. 3 (2015) 1096–1101.

[38] K. Song, J. Zhang, Y. Liu, C. Zhang, J. Jiang, H. Jiang, H.B. Qin, A red-emitting phosphor $Ba_9Lu_2Si_6O_{24}$:Ce^{3+}, Mn^{2+} with enhanced energy transfer via self-charge compensation, J. Phy. Chem. C 119 (2015) 24558–24563.

[39] L.H. Wang, L.F. Schneemeyer, R.J. Cava, T. Siegrist, A new barium scandium silicate: $Ba_9Sc_2(SiO_4)_6$, J. Solid State Chem. 113 (1994) 211–214.

[40] R.T. Shannon, Revised effective ionic radii and systematic studies of interatomic distances in halides and chalcogenides, Acta Cryst. A 32 (1976) 751–767.

[41] D.T. Palumbo, J.J. Brown, Electronic states of Mn^{2+}-activated phosphors: I. green-emitting phosphors, J. Electrochem. Soc. 117 (1970) 1184–1188.

[42] Y. Zhang, X. Li, K. Li, H. Lian, M. Shang, J. Lin, Crystal-site engineering control for the reduction of Eu^{3+} to Eu^{2+} in $CaYAlO_4$: structure refinement and tunable emission properties, ACS Appl. Mater. Interfaces 7 (2015) 2715–2725.

[43] T.C. Ozawa, K. Fukuda, K. Akatsuka, Y. Ebina, T. Sasaki, Preparation and characterization of the Eu^{3+} doped perovskite nanosheet phosphor: $La_{0.90}Eu_{0.05}Nb_2O_7$, Chem. Mater. 19 (2007) 6575–6580.

[44] Y. Liu, X. Zhang, Z. Hao, Y. Luo, X. Wang, L. Ma, J. Zhang, Luminescence and energy transfer in $Ca_3Sc_2Si_3O_{12}$:Ce^{3+}, Mn^{2+} white LED phosphors, J. Lumin. 133 (2013) 21–24.

[45] X. Zhang, J. Wang, L. Huang, F. Pan, Y. Chen, B. Lei, M. Peng, M. Wu, Tunable luminescent properties and concentration-dependent: site-preferable distribution of Eu^{2+} ions in silicate glass for white LEDs applications, ACS Appl. Mater. Interfaces 7 (2015) 10044–10054.